Determination of Iron−Ligand Bond Lengths in Horse Heart Met- and Deoxymyoglobin Using Multiple-Scattering XAFS Analyses

Anne M. Rich, Robert S. Armstrong,* Paul J. Ellis, Hans C. Freeman, and Peter A. Lay*

School of Chemistry, University of Sydney, Sydney, New South Wales 2006, Australia

Received November 18, 1997

XAFS data in the range $0 \leq k \leq 14.5$ Å^{-1} have been obtained from frozen aqueous solutions (10 K) of horse heart myoglobin (Mb) in the Fe(III) (aqua-met) and Fe(II) (deoxy) forms. The structures of the Fe sites have been refined using both single-scattering (SS) and multiple-scattering (MS) analyses. The XAFS MS analyses yield more precise Fe−ligand bond lengths (estimated error 0.02−0.03 Å) than those determined crystallographically (estimated errors ≥0.1 Å). For met-Mb, the MS analysis results in an average Fe−N(pyrrole) distance of 2.05 Å, an Fe−N(imidazole) distance of 2.17 Å, and an Fe−O(aqua) distance of 2.08 Å. For deoxy-Mb, the MS analysis results in Fe−N(pyrrole) and Fe−N(imidazole) distances of 2.06 and 2.16 Å, respectively. The final XAFS *R* values are 18.8% and 17.8% for met- and deoxy-Mb, respectively. The robustness of the refinements was tested by varying the starting models, constraints, restraints, and *k* ranges.

Introduction

Myoglobin (Mb) is a small protein (17.6 kDa) consisting of a single polypeptide chain of 153 amino acid residues and a protoporphyrin IX (heme) prosthetic group. It functions in cardiac muscle to store oxygen (O_2) and to facilitate its diffusion from blood capillaries to the mitochondria.[1,2] The heme is linked to the protein by a covalent bond from the iron atom to an imidazole nitrogen (N_ϵ) of the proximal histidine. In vivo, the iron atom is maintained in the ferrous (Fe(II)) state, being high-spin five-coordinate in deoxy-Mb and low-spin six-coordinate in oxy-Mb, where the sixth position is occupied by O_2. In vitro, O_2 causes the autoxidation of oxy-Mb to met-Mb in which the iron atom is high-spin ferric (Fe(III)) and the sixth ligand is water.[1,2]

Sperm whale (*Physeter catodon*) met-Mb was the first protein for which a complete 3-dimensional crystal structure was determined.[3] Takano subsequently reported the first refinements of the sperm whale met-Mb and deoxy-Mb structures at 2.0 Å resolution.[4,5] More recent refinements have yielded structures of sperm whale met-Mb and deoxy-Mb at resolutions ranging from 1.4 to 2.0 Å (Table 1).[6,7] Other species for which the crystal structures of met-Mb have been reported are horse heart (*Equus caballus*; 1.9 Å resolution),[8] common seal (*Phoca vitulina*; 2.5 Å),[9] sea hare (*Aplysia limacina*; 1.6 Å),[10] pig (*Sus scrofa*; 1.75 Å),[11] loggerhead sea turtle (*Caretta caretta*; 2.0 Å),[12] and yellowfin tuna (*Thunnus albacares*; 1.74 Å).[13]

XAFS spectroscopy has the capacity to probe the structure around the Fe atom with higher precision than that accessible, until recently, by protein crystallography.[14,15] Under favorable conditions, XAFS analyses of metalloproteins yield distances accurate to 0.01−0.02 Å.[15] A recent development has been the use of ab initio multiple-scattering (MS) calculations instead of the earlier single-scattering (SS) analyses using the plane-wave approximation and empirically derived amplitudes and phase shifts. MS processes involving three or more atoms are important in determining the XAFS contributions of distant shells and become particularly important at low *k* values or in cases where three atoms are approximately collinear.[16,17] The effects drop off very rapidly for intervector angles smaller than ∼150°. In heme proteins, atoms up to 5 Å from the Fe center may make significant MS contributions. This distance generally captures all of the atoms of the porphyrin core and any exogenous ligand.[18]

Heme proteins for which SS XAFS analyses have been reported include sperm whale Mb[19−22] and hemoglobin.[18] Here we report MS XAFS analyses of horse heart met- and deoxy-

(1) Antonini, E.; Brunori, M. *Hemoglobin and Myoglobin in Their Reactions with Ligands*; North-Holland: Amsterdam, 1971; Vol. 21.
(2) *Hemoglobins*; Antonini, E., Rossi-Bernardi, L., Chiancone, E., Eds.; Methods in Enzymology, Vol. 76; Academic Press: New York, 1981.
(3) Kendrew, J. C.; Dickerson, R. E.; Strandberg, B. E.; Hart, R. G.; Davies, D. R.; Phillips, D. C.; Shore, V. C. *Nature (London)* **1960**, *185*, 422−427.
(4) Takano, T. *J. Mol. Biol.* **1977**, *110*, 537−568.
(5) Takano, T. *J. Mol. Biol.* **1977**, *110*, 569−584.
(6) Phillips, S. E. V. Unpublished work. PDB entry 1MBD.
(7) Yang, F.; Phillips, G. N., Jr. *J. Mol. Biol.* **1996**, *256*, 762−774.
(8) Evans, S. V.; Brayer, G. D. *J. Mol. Biol.* **1990**, *213*, 885−897.
(9) Scouloudi, H.; Baker, E. N. *J. Mol. Biol.* **1978**, *126*, 637−660.
(10) Bolognesi, M.; Onesti, S.; Gatti, G.; Coda, A.; Ascenzi, P.; Brunori, M. *J. Mol. Biol.* **1989**, *205*, 529−544.
(11) Oldfield, T. J.; Smerdon, S. J.; Dauter, Z.; Petratos, K.; Wilson, K. S.; Wilkinson, A. J. *Biochemistry* **1992**, *31*, 8732−8739.
(12) Nardini, M.; Tarricone, C.; Rizzi, M.; Lania, A.; Desideri, A.; Sanctis, G. D.; Coletta, M.; Petruzzelli, R.; Ascenzi, P.; Coda, A.; Bolognesi, M. *J. Mol. Biol.* **1995**, *247*, 459−465.
(13) Birnbaum, G. I.; Evans, S. V.; Przybylska, M.; Rose, D. R. *Acta Crystallogr., Sect. D* **1994**, *D50*, 283−289.
(14) Chance, M. R.; Parkhurst, L. J.; Powers, L. S.; Chance, B. *J. Biol. Chem.* **1986**, *261*, 5689−5692.
(15) Gurman, S. J. *J. Synchrotron Rad.* **1995**, *2*, 56−63.
(16) Teo, B.-K. *J. Am. Chem. Soc.* **1981**, *103*, 3990−4001.
(17) Teo, B.-K. In EXAFS and Near Edge Structure; Bianconi, A., Inoccia, L., Stipcich, S., Eds.; Springer-Verlag: Berlin, Heidelberg, 1983; pp 11−21.
(18) Pin, S.; Alpert, B.; Congiu-Castellano, A.; Longa, S. D.; Bianconi, A. *Hemoglobins*; Methods in Enzymology, Vol. 232; Academic Press: New York, 1994; Part C, pp 266−292.
(19) Quillin, M. L.; Arduini, R. M.; Olson, J. S.; Phillips, G. N., Jr. *J. Mol. Biol.* **1993**, *234*, 140−155; crystals cooled to 0 °C.
(20) Quillin, M. L.; Li, T.; Olson, J. S.; Phillips, G. N., Jr.; Dou, Y.; Ikeda-Saito, M.; Regan, R.; Carlson, M.; Gibson, Q. H.; Li, H.; Elber, R. *J. Mol. Biol.* **1995**, *245*, 416−436; crystals cooled to 0−4 °C.
(21) Teng, T.-Y.; Huang, H. W.; Olah, G. A. *Biochemistry* **1987**, *26*, 8066−8072.

10.1021/ic9714549 CCC: $15.00
Published on Web 10/13/1998

Table 1. Summary of Crystallographic Data for Sperm Whale and Horse Heart Met- and Deoxy-Mb

protein	pH	d_{min}[a] (Å)	N[b]	no. of *F*s[c]	*C*[d]	*R*[e]	bond lengths (Å) Fe−N_p(av)	Fe−N_ϵ	Fe−OH_2	range of Fe−N_P (Å)	$\sigma_w(x)$[f] (Å)	ref	PDB[g] entry
met-Mb													
sperm whale	5.75	2.0	1383	9017	n/a	0.172	2.04	2.17	2.10	0.14	0.23[h]	4	4MBN
sperm whale	4.0	2.0	1418	7156	0.826	0.200	1.91	2.50	2.25	0.38	0.42	7	1VXB
horse heart	n/a	1.9	1401	6035	0.616	0.155	2.01	2.26	2.29	0.07	0.40	8	1YMB
sperm whale	5.0	1.7	1404	13807	0.976	0.156	2.01	2.10	2.11	0.08	0.11	7	1VXE
sperm whale	6.0	1.7	1454	13856	0.979	0.140	1.99	2.15	2.17	0.10	0.10	7	1VXH
deoxy-Mb													
sperm whale	5.75	2.0	1382	8788	n/a	0.179	2.07	2.17		0.18	0.24[h]	5	5MBN
sperm whale	4.0	2.0	1377	7235	0.841	0.177	1.90	2.20		0.14	0.34	7	1VXA
sperm whale	5.0	1.7	1430	13882	0.980	0.153	1.98	2.28		0.04	0.11	7	1VXD
sperm whale	6.0	1.7	1434	12785	0.900	0.157	1.95	2.31		0.08	0.13	7	1VXG
sperm whale	8.4	1.4	1667	26428[i]	1.000[i]	0.175[i]	2.02	2.10		0.12	0.07	6	1MBD

[a] d_{min} = resolution of data. [b] *N* = number of atoms. [c] no. of *F* 's = number of independent X-ray reflections included in the refinement of the crystal structure. [d] *C* = completeness of data = number of independent X-ray reflections included in the refinement, expressed as a fraction of the number of reflections theoretically accessible in the resolution range of the data. [e] *R* = crystallographic residual. [f] $\sigma_w(x)$ = diffraction precision indicator (DPI) = uncertainty in the position of an average atom.[44] $\sigma_w(x) = 1.0(N/P)^{1/2}C^{-1/3}d_{min}R$, where *P* = number of degrees of freedom = (number of independent reflections − number of variables). If the positional coordinates *x*, *y*, *z* and the isotropic displacement parameter *B* of each atom are refined, the number of variables = 4*N*. [g] PDB = Brookhaven Protein Data Bank.[55] [h] Assumes *C* (completeness of data) = 0.95. [i] Personal communication from Professor S. E. V. Phillips.

Mb. The new Fe−ligand distances are compared with values obtained by X-ray crystallography, antecedent SS XAFS analyses, and SS analyses of our own XAFS data.

Experimental Section

Sample Preparation and Data Collection. Horse heart Mb (Sigma) was purified by chromatography on a Whatman CM-32 column at 4 °C using a phosphate buffer solution (5 mM NaH_2PO_4; 6.6 mM NaH_2PO_4, pH 7) as the eluent. The Mb thus obtained was dialyzed against distilled water and was concentrated using Amicon ultrafiltration cells. The concentrations of Mb were estimated spectroscopically for met-Mb in 0.1 M phosphate buffer (pH 6.8) using the following molar absorptivities: $\epsilon_{280} = 3.37 \times 10^4$ M^{-1} cm^{-1}; $\epsilon_{408} = 1.6 \times 10^5$ M^{-1} cm^{-1}; and $\epsilon_{505} = 1.02 \times 10^4$ M^{-1} cm^{-1}.[23] Deoxy-Mb was prepared in a septum-crimped vial by reduction of met-Mb with deoxygenated (Ar) aqueous sodium dithionite (Fluka, ~95:5% $Na_2S_2O_4/H_2O$; dried and stored over P_2O_5 in the dark) using syringe techniques on an Ar line. The resulting final concentrations of the freshly prepared solutions were 4.1 and 3.2 mM for met-Mb and deoxy-Mb, respectively, after glycerol (AR grade, Ar-degassed in the case of deoxy-Mb) was added to produce a 40% v/v glycerol/water mixture. This glycerol concentration was the minimum required to form a homogeneous glass upon freezing. The solutions were syringed into 140-μL Lucite XAFS cells (23 × 2 × 3 mm) with 63.5-μm Mylar tape windows. This operation was conducted in a nitrogen-filled glovebag. Immediately after their preparations, the samples were frozen in a liquid nitrogen/*n*-hexane slurry.

X-ray absorption spectra were recorded at the Stanford Synchrotron Radiation Laboratory (SSRL) on the unfocused beamline 7-3 (3 GeV, 95−55 mA), using a Si(220) double-crystal monochromator detuned 50% at 7993 eV to minimize harmonic contamination. Data were collected as fluorescence spectra using a 13-element Ge array detector.[24] For each sample, 12−22 scans were recorded from 6790 to 7990 eV. In the case of met-Mb, the sample cell was moved whenever photoreduction was apparent, to expose a fresh portion of protein to the beam. A constant temperature of 10 K was maintained using an Oxford Instruments continuous-flow liquid-helium CF 1208 cryostat. The energy was calibrated using an Fe foil standard, assigning the first inflection point to an energy of 7111.2 eV.[25]

The scans for each protein were averaged using weights based on the signal-to-noise ratios, and monochromator glitches were removed.

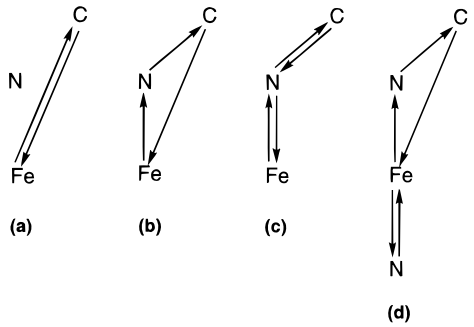

Figure 1. Examples of paths contributing to the XAFS in a four-atom system: (a) single-scattering (two legs); (b) multiple-scattering (three legs); (c) multiple-scattering (four legs); (d) multiple-scattering (five legs).

A background correction was applied by fitting a third-order polynomial to the pre-edge region, extrapolating it into the XAFS region, and subtracting it from the data. A three-region spline was fitted to the XAFS region and was then subtracted. The data were normalized to an edge jump of 1.0 (where the edge jump denotes the underlying intensity of the edge after subtracting the XAFS) and were compensated for decreasing absorbance past the edge. The background-subtracted, normalized and compensated data were converted to *k* space, where *k* is the photoelectron wavevector, $\hbar^{-1}[2m_e(E - E_0)]^{1/2}$, where $\hbar$ is $h/2\pi$, m_e is the mass of the electron, E_0 is the threshold energy for the $1s \rightarrow$ continuum transition, and $E - E_0$ is the energy of the photoelectron generated.[15]

Definition of Terms. Several terms used in the following discussion require definition. The XAFS ($\chi(k)$) is the sum of contributions from many scattering *paths* (Figure 1). Each path is a route by which a photoelectron may proceed from the absorber to neighboring atoms and back to the absorber. The step from one atom to the next along a path is called a *leg*. The *effective length* of a path is half the total distance traveled by the photoelectron (for SS this is the absorber−scatterer distance). The *importance factor* of a path is defined as

$$\int_{k=0}^{20} |\chi(k)|\, dk$$

The final *k* values for met- and deoxy-Mb were 15.0 and 14.5 $Å^{-1}$, respectively. Although the importance factors are calculated by the program FEFF 6.01,[26] these they do not include the effects of the

(22) Zhang, K.; Reddy, K. S.; Bunker, G.; Chance, B. *Proteins: Struct., Funct., Genet.* **1991**, *10*, 279−286.
(23) *Handbook of Biochemistry and Molecular Biology*, 3rd ed.; CRC Press: Cleveland, OH, 1976; Vol. II.
(24) Cramer, S. P.; Tench, O.; Yocum, M.; George, G. N. *Nucl. Instrum. Methods Phys. Res., Sect. A* **1988**, *A266*, 586−591.
(25) Zhang, Y.; Pavlosky, M. A.; Brown, C. A.; Westre, T. E.; Hedman, B.; Hodgson, K. O.; Solomon, E. I. *J. Am. Chem. Soc.* **1992**, *114*, 9189−9191.

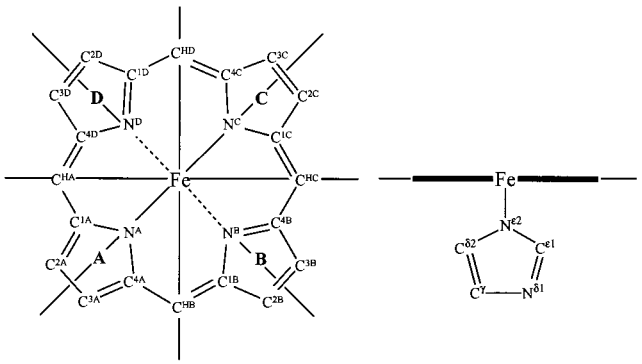

Figure 2. Molecular structure of the TPP model used in MS XAFS analyses, viewed from the distal side of the heme pocket. The atoms are labeled according to the Brookhaven Data Bank convention.[55] The model includes all non-H atoms of the imidazole ring and porphyrin ligands within 5 Å of the Fe atom. The sixth position may be left vacant (as in the deoxy adduct) or occupied by ligands such as H_2O (as in the met form).

temperature factors ($e^{-2\sigma^2}$), whereas the XFIT program does.[27,28] This program multiplies the importance factors by the temperature factor of each atom along a path. Therefore, the longer a path and the larger the number of atoms along it, the lower are the values of the importance factors and the calculated contribution to the scattering intensity.

XFIT Data Analysis. The model-fitting calculations were performed by means of the program XFIT.[27,28] In this program, a nonlinear least-squares procedure is used to fit the model parameters to the observed XAFS.[27] XFIT incorporates ab initio calculations of the XAFS using the programs FEFF 4.06[29] for SS and FEFF 6.01[26] for MS. The parameters that were varied in order to optimize the agreement between the observed and calculated XAFS were the coordinates *x*, *y*, *z* of all atoms in the model in relation to an arbitrary set of Cartesian axes, the Debye−Waller factors σ^2, a scale factor S_0^2, and E_0. Both the observed and calculated XAFS were Fourier filtered.[27] The *k* windows used for the XAFS analyses are shown in the figures. The goodness-of-fit parameter *R* was calculated as described by Ellis and Freeman.[27] The statistical errors in the final parameters arising from the noise in the data were estimated by Monte Carlo analyses.[27]

Two Models for the Fe Site in Myoglobin. To assess the extent of model bias in the XFIT analyses, two different models were used to initiate the calculations. The first model (PP-IX model) comprised all non-H atoms of the ImH ring of the 1-methylimidazole (1-MeImH) and protoporphyrin IX (PP-IX) ligands within 5 Å of the Fe atom in $[Fe(1\text{-}MeImH)_2(PP\text{-}IX)]CH_3OH{\cdot}H_2O$[30] (Figure 2). In the second model (TPP model, where TPP = *meso*-tetraphenylporphyrinato(2−)), the porphyrin dimensions (excluding those of the phenyl substituents) were taken from a consensus structure for 6-coordinate Fe(TPP) complexes,[31] while the dimensions of the coordinated imidazole were typical values found in, e.g., the crystal structure of $[Mn(ImH)_6]Cl_2{\cdot}4H_2O$.[32] The TPP model has been shown to reproduce accurately the X-ray crystal structures of Fe−porphyrin model complexes.[33] While the PP-IX model was more closely related to the heme group of Mb, the TPP model introduced fewer variables because of its higher symmetry (see Tables 2 and 3).

Table 2. Constraints and Restraints Used in the Refinements of met- and deoxy-Mb, Using the TPP Model

Debye−Waller Factor Restraints[a]

$\sigma^2_{C1A} > (\sigma^2_{NA} + 0.002)$ {0.001}
$\sigma^2_{CHA} > (\sigma^2_{C1A} + 0.002)$ {0.001}
$\sigma^2_{C2A} > (\sigma^2_{C1A} + 0.002)$ {0.001}
$\sigma^2_{N\delta1} > (\sigma^2_{N\epsilon2} + 0.002)$ {0.001}
$\sigma^2_{C\epsilon1} > (\sigma^2_{N\delta1} + 0.002)$ {0.001}
$\sigma^2_i > 0.001$ {0.0005} for all *i*
$\sigma^2_i < 0.08$ {0.01} for all *i*

Debye−Waller Factor Constraints

$\sigma^2_{NA} = \sigma^2_{NC} = \sigma^2_{ND} = \sigma^2_{NB}$
σ^2_{Ci} is the same where *i* = 1A, 4A, 1B, 4B, 1C, 4C, 1D, 4D

$\sigma^2_{CHB} = \sigma^2_{CHA} = \sigma^2_{CHD} = \sigma^2_{CHC}$
σ^2_{Ci} is the same where *i* = 2A, 3A, 2B, 3B, 2C, 3C, 2D, 3D

$\sigma^2_{C\epsilon1} = \sigma^2_{C\delta2}$
$\sigma^2_{N\delta1} = \sigma^2_{C\gamma}$

Bond Length Restraints

N(A)−C(1A) ≈ 1.384 Å {0.01}
N(A)−C(4A) ≈ 1.384 Å {0.01}
C(1A)−C(HA) ≈ 1.393 Å {0.02}
C(4A)−C(HB) ≈ 1.393 Å {0.02}
C(1A)−C(2A) ≈ 1.439 Å {0.01}
C(3A)−C(4A) ≈ 1.439 Å {0.01}
C(2A)−C(3A) ≈ 1.341 Å {0.01}
$N^{\epsilon2}-C^{\epsilon1} \approx 1.317$ Å {0.01}
$N^{\epsilon2}-C^{\delta2} \approx 1.371$ Å {0.01}
$C^{\epsilon1}-N^{\delta1} \approx 1.336$ Å {0.01}
$C^{\delta2}-C^{\gamma} \approx 1.347$ Å {0.01}
$N^{\delta1}-C^{\gamma} \approx 1.346$ Å {0.01}

Bond Angle Restraints

C(1A)−N(A)−C(4A) ≈ 105.2° {1}
N(A)−C(1A)−C(2A) ≈ 110.1° {1}
N(A)−C(4A)−C(3A) ≈ 110.1° {1}
N(A)−C(1A)−C(HA) ≈ 125.6° {2}
N(A)−C(4A)−C(HB) ≈ 125.6° {2}
C(1A)−C(2A)−C(3A) ≈ 107.3° {1}
C(2A)−C(3A)−C(4A) ≈ 107.3° {1}
C(1A)−C(HA)−C(4D) ≈ 124.0° {2}
$C^{\epsilon1}-N^{\epsilon2}-C^{\delta2} \approx 104.8°$ {1}
$N^{\epsilon2}-C^{\delta2}-C^{\gamma} \approx 109.8°$ {1}
$N^{\epsilon2}-C^{\epsilon1}-N^{\delta1} \approx 111.4°$ {1}
$C^{\delta2}-C^{\gamma}-N^{\delta1} \approx 106.3°$ {1}
$C^{\epsilon1}-N^{\delta1}-C^{\gamma} \approx 107.7°$ {1}

Symmetry Constraints

$z_i = 0$ for *i* = all pyrrole and *meso* atoms
$x_{NC} = y_{NB} = -x_{NA}$
$y_{ND} = x_{NA}$
$y_{NA} = y_{NC} = 0$
$x_{ND} = x_{NB} = 0$
$x_{C4D} = y_{C1A}$; $y_{C4D} = x_{C1A}$
$x_{C1D} = -x_{C4D}$; $y_{C1D} = y_{C4D}$
$x_{C4C} = -x_{C1A}$; $y_{C4C} = y_{C1A}$
$x_{C1C} = x_{C4C}$; $y_{C1C} = -y_{C4C}$
$x_{C4B} = x_{C1D}$; $y_{C4B} = -y_{C1D}$
$x_{C1B} = -x_{C4B}$; $y_{C1B} = y_{C4B}$
$x_{C4A} = x_{C1A}$; $y_{C4A} = -y_{C1A}$
$x_{CHB} = -y_{CHB}$
$x_{CHA} = x_{CHB}$
$y_{CHA} = x_{CHA}$
$x_{CHD} = -x_{CHA}$
$y_{CHD} = -x_{CHD}$
$x_{CHC} = -x_{CHB}$
$y_{CHC} = y_{CHB}$
$x_{C3B} = y_{C2C}$; $y_{C3B} = x_{C2C}$
$x_{C2B} = -x_{C3B}$; $y_{C2B} = y_{C3B}$
$x_{C3A} = -x_{C2C}$; $y_{C3A} = y_{C2C}$
$x_{C2A} = x_{C3A}$; $y_{C2A} = -y_{C3A}$
$x_{C2D} = y_{C2A}$; $y_{C2D} = x_{C2A}$
$x_{C2D} = -x_{C3D}$; $y_{C2D} = y_{C3D}$
$x_{C2C} = x_{C3C}$; $y_{C2C} = -y_{C3C}$
$y_{N\epsilon2} = y_{C\epsilon1} = y_{C\delta2} = y_{N\delta1} = y_{C\gamma} = 0$
$x_{N\epsilon2} = 0$
$Fe-N^{\epsilon2}-C^{\epsilon1} = Fe-N^{\epsilon2}-C^{\delta2}$

[a] The quantities in the braces {} are the values of σ_{res} as defined in the text.

Restrictions on Multiple-Scattering Paths. As a practical measure, the MS refinement calculations for met- and deoxy-Mb were restricted to paths with an effective length ≤5.0 Å, not more than five legs, and an importance factor ≥2% compared with the most important path (Fe→N_p→Fe). There were approximately 150 such paths (∼50% of the total number) for the TPP model and approximately 550 (∼20% of the total number) for the PP-IX model. A repetition of the refinements including all paths with an effective length ≤5.1 Å and up to six legs[34] produced identical values for the Fe−ligand bond lengths, confirming that the restrictions on the number of paths had not affected these results.

(26) Rehr, J. J.; Albers, R. C.; Zabinsky, S. I. *Phys. Rev. Lett.* **1992**, *69*, 3397−3400.
(27) Ellis, P. J.; Freeman, H. C. *J. Synchrotron Rad.* **1995**, *2*, 190−195.
(28) *XFIT for Windows '95*; Australian Synchrotron Research Program: Sydney, 1996.
(29) Mustre de Leon, J.; Rehr, J. J.; Zabinsky, S. I.; Albers, R. C. *Phys. Rev. B* **1991**, *44*, 4146−4156.
(30) Little, R. G.; Dymock, K. R.; Ibers, J. A. *J. Am. Chem. Soc.* **1975**, *97*, 4532−4539.
(31) The bond distances and angles for the MS XAFS model were taken from Scheidt and Lee (Scheidt, W. R.; Lee, Y. J. *Struct. Bonding (Berlin)* **1987**, *64*, 1−70) and were the averages of values in a number of Fe(TPP) complexes (Mashiko, T.; Reed, C. A.; Haller, K. J.; Scheidt, W. R. *Inorg. Chem.* **1984**, *23*, 3192−3196). The complexes contributing to the averages were $[Fe(THT)_2(TPP)]{\cdot}THT$, $[Fe(PMS)_2(TPP)]^+$, and $[Fe(C_5Im)(TPP)(THT)]{\cdot}C_6H_6$ (Mashiko, T.; Reed, C. A.; Haller, K. J.; Kastner, M. E.; Scheidt, W. R. *J. Am. Chem. Soc.* **1981**, *103*, 5758−5767) and $[Fe(Pip)_2(TPP)]$ (Radonovich, L. J.; Bloom, A.; Hoard, J. L. *J. Am. Chem. Soc.* **1972**, *94*, 2073−2078).
(32) Garrett, T. P. J.; Guss, J. M.; Freeman, H. C. *Acta Crystallogr., Sect. C* **1983**, *C39*, 1027−1031.
(33) Ellis, P. J.; Freeman, H. C.; Hedman, B.; Hodgson, K. O.; Ibers, J. A.; Shi, D.; Slebodnick, C. To be published.

Table 3. Constraints and Restraints Used in the Refinements of met- and deoxy-Mb, Using the PP-IX Model

Debye−Waller Factor Restraints[a]

$\sigma^2_{C1A} > (\sigma^2_{NA} + 0.002)$ {0.001}
$\sigma^2_{CHA} > (\sigma^2_{C1A} + 0.002)$ {0.001}
$\sigma^2_{C2A} > (\sigma^2_{C1A} + 0.002)$ {0.001}
$\sigma^2_{N\delta1} > (\sigma^2_{N\epsilon2} + 0.002)$ {0.001}
$\sigma^2_{C\epsilon1} > (\sigma^2_{N\delta1} + 0.002)$ {0.001}
$\sigma^2_i > 0.002$ {0.001} for all i
$\sigma^2_i < 0.02$ {0.01} for all i

Debye−Waller Factor Constraints

$\sigma^2_{NA} = \sigma^2_{NB} = \sigma^2_{NC} = \sigma^2_{ND}$
σ^2_{Ci} is the same where i = 1A, 4A, 1B, 4B, 1C, 4C, 1D, 4D

$\sigma^2_{CHA} = \sigma^2_{CHB} = \sigma^2_{CHC} = \sigma^2_{CHD}$
σ^2_{Ci} is the same where i = 2A, 3A, 2B, 3B, 2C, 3C, 2D, 3D

$\sigma^2_{C\epsilon1} = \sigma^2_{C\delta2}$
$\sigma^2_{N\delta1} = \sigma^2_{C\gamma}$

Bond Length Restraints

N(A)−C(1A) ≈ 1.380 Å {0.01}
N(A)−C(4A) ≈ 1.368 Å {0.01}
N(B)−C(1B) ≈ 1.377 Å {0.01}
N(B)−C(4B) ≈ 1.371 Å {0.01}
N(C)−C(1C) ≈ 1.381 Å {0.01}
N(C)−C(4C) ≈ 1.373 Å {0.01}
N(D)−C(1D) ≈ 1.373 Å {0.01}
N(D)−C(4D) ≈ 1.371 Å {0.01}
C(1A)−C(2A) ≈ 1.449 Å {0.01}
C(1B)−C(2B) ≈ 1.465 Å {0.01}
C(1C)−C(2C) ≈ 1.412 Å {0.01}
C(1D)−C(2D) ≈ 1.453 Å {0.01}
C(1A)−C(HA) ≈ 1.377 Å {0.01}
C(1B)−C(HB) ≈ 1.360 Å {0.01}
C(1C)−C(HC) ≈ 1.378 Å {0.01}
C(1D)−C(HD) ≈ 1.333 Å {0.01}
C(2A)−C(3A) ≈ 1.354 Å {0.01}
C(2B)−C(3B) ≈ 1.330 Å {0.01}
C(2C)−C(3C) ≈ 1.345 Å {0.01}
C(2D)−C(3D) ≈ 1.349 Å {0.01}
C(3A)−C(4A) ≈ 1.433 Å {0.01}
C(3B)−C(4B) ≈ 1.478 Å {0.01}
C(3C)−C(4C) ≈ 1.420 Å {0.01}
C(3D)−C(4D) ≈ 1.452 Å {0.01}
C(4A)−C(HB) ≈ 1.381 Å {0.01}
C(4B)−C(HC) ≈ 1.347 Å {0.01}
C(4C)−C(HD) ≈ 1.377 Å {0.01}
C(4D)−C(HA) ≈ 1.385 Å {0.01}
$r_{NA} \approx r_{NB} \approx r_{NC} \approx r_{ND}$ {0.005}
$N^{\epsilon2}-C^{\epsilon1} \approx 1.326$ Å {0.01}
$N^{\epsilon2}-C^{\delta2} \approx 1.368$ Å {0.01}
$C^{\epsilon1}-N^{\delta1} \approx 1.338$ Å {0.01}
$C^{\delta2}-C^{\gamma} \approx 1.347$ Å {0.01}
$N^{\delta1}-C^{\gamma} \approx 1.354$ Å {0.01}

Bond Angle Restraints

N(A)−C(1A)−C(2A) ≈ 110.8° {1}
N(A)−C(4A)−C(3A) ≈ 111.7° {1}
N(A)−C(1A)−C(HA) ≈ 125.2° {3}
N(A)−C(4A)−C(HB) ≈ 122.8° {3}
N(B)−C(1B)−C(HB) ≈ 124.6° {3}
N(B)−C(1B)−C(2B) ≈ 109.4° {1}
N(B)−C(4B)−C(HC) ≈ 125.9° {3}
N(B)−C(4B)−C(3B) ≈ 108.3° {1}
N(C)−C(1C)−C(HC) ≈ 124.9° {3}
N(C)−C(1C)−C(2C) ≈ 110.7° {1}
N(C)−C(4C)−C(HD) ≈ 125.0° {3}
N(C)−C(4C)−C(3C) ≈ 108.6° {1}
N(D)−C(1D)−C(HD) ≈ 125.3° {3}
N(D)−C(4D)−C(HA) ≈ 125.1° {3}
N(D)−C(1D)−C(2D) ≈ 109.0° {1}
N(D)−C(4D)−C(3D) ≈ 110.6° {1}
C(1A)−N(A)−C(4A) ≈ 104.5° {1}
C(1A)−C(HA)−C(4D) ≈ 125.4° {3}
C(1A)−C(2A)−C(3A) ≈ 106.3° {1}
C(2A)−C(3A)−C(4A) ≈ 106.7° {1}
C(2A)−C(1A)−C(HA) ≈ 123.8° {1}
C(3A)−C(4A)−C(HB) ≈ 124.5° {1}
C(4A)−C(HB)−C(1B) ≈ 127.5° {3}
C(1B)−N(B)−C(4B) ≈ 107.4° {1}
C(1B)−C(2B)−C(3B) ≈ 106.8° {1}
C(2B)−C(3B)−C(4B) ≈ 108.1° {1}
C(2B)−C(1B)−C(HB) ≈ 126.0° {1}
C(3B)−C(4B)−C(HC) ≈ 125.8° {1}
C(4B)−C(HC)−C(1C) ≈ 125.7° {3}
C(1C)−N(C)−C(4C) ≈ 105.8° {1}
C(1C)−C(2C)−C(3C) ≈ 105.9° {1}
C(2C)−C(3C)−C(4C) ≈ 109.1° {1}
C(2C)−C(1C)−C(HC) ≈ 124.4° {1}
C(3C)−C(4C)−C(HD) ≈ 126.4° {1}
C(4C)−C(HD)−C(1D) ≈ 125.7° {3}
C(1D)−N(D)−C(4D) ≈ 106.4° {1}
C(1D)−C(2D)−C(3D) ≈ 108.2° {1}
C(2D)−C(3D)−C(4D) ≈ 105.8° {1}
C(2D)−C(1D)−C(HD) ≈ 125.6° {1}
C(3D)−C(4D)−C(HA) ≈ 124.1° {1}
$C^{\epsilon1}-N^{\epsilon2}-C^{\delta2} \approx 104.9°$ {1}
$N^{\epsilon2}-C^{\delta2}-C^{\gamma} \approx 109.8°$ {1}
$N^{\epsilon2}-C^{\epsilon1}-N^{\delta1} \approx 111.4°$ {1}
$C^{\delta2}-C^{\gamma}-N^{\delta1} \approx 106.8°$ {1}
$C^{\epsilon1}-N^{\delta1}-C^{\gamma} \approx 107.1°$ {1}

Symmetry Constraints

$z_i = 0$ for all pyrrole and *meso* atoms
$y_{NA} = 0$
$x_{NA} = -x_{NC} = y_{ND} = -y_{NB}$
$y_{N\epsilon2} = y_{C\epsilon1} = y_{C\delta2} = y_{N\delta1} = y_{C\gamma} = 0$
$x_{N\epsilon2} = 0$
$Fe-N^{\epsilon2}-C^{\epsilon1} = Fe-N^{\epsilon2}-C^{\delta2}$

[a] The quantities in the braces {} are the values of σ_{res} as defined in the text.

Constraints and Restraints in XFIT Refinements. Constraints and restraints were used to incorporate prior structural information in the analyses and to reduce the degrees of freedom in the models[27] (Tables 2 and 3). Constraints specify precise relationships between parameters; restraints specify targets for relationships between parameters. In XFIT, the weight of each restraint expression is specified by $1/\sigma_{res}^2$, where the parameter σ_{res} is analogous to an estimated standard deviation (esd). The weight of the XAFS data relative to the restraints was governed by a separate weighting factor, w. In a series of preliminary refinements, it was determined that a value of $w = 8$ resulted in errors between refined and ideal values of geometrical parameters close to the specified σ_{res} values. The bond lengths and bond angles within the porphyrin ligand were tightly restrained to the geometry of the model (σ_{res} = 0.01 Å and 1° for bond lengths and bond angles, respectively). Weaker restraints were placed on the bond lengths and angles at the *meso* sites to permit the pyrrole rings to move closer to or further away from the Fe atom (σ_{res} = 0.02 Å and 2°, respectively). In the final models, the errors in the restrained bond lengths and angles were ≤0.01 Å and ≤1°, respectively.

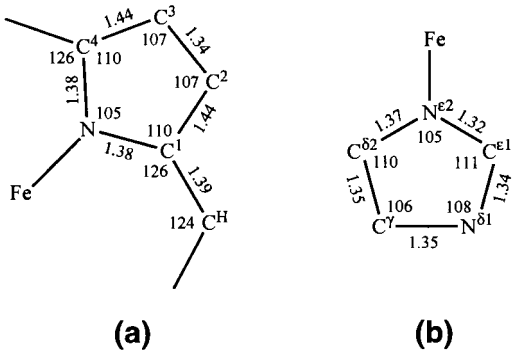

Figure 3. Dimensions used in the bond length and bond angle restraints in the multiscattering analyses: (a) pyrrole ring of the TPP model; (b) imidazole ring of the proximal histidine. The quasi-esds used as weights for the restraints were 0.01 Å and 1° for the bond lengths and angles, respectively (0.02 Å and 2° for the *meso*-C's).

All Debye−Waller factors, σ^2, were restrained to be positive and below 0.08 Å^2. The values of σ^2 in the porphyrin ring were restrained to increase by 0.001 Å^2 per bond away from the Fe atom. This pattern reflected the expected increase in static and dynamic disorder as the distance of the scatterer from the absorber increases.[35] For the histidine imidazole ring, the Debye−Waller factors were restrained to increase in the order $\sigma^2(N^{\epsilon2}) < \sigma^2(N^{\delta1}, C^{\gamma}) < \sigma^2(C^{\epsilon1}, C^{\delta2})$ with σ_{res} = 0.001 Å^2 (see atom labels in Figure 2). The irregular order of the Debye−Waller factors reflects the fact that in-plane rocking vibrational modes have a greater effect on the $Fe-C^{\epsilon1}$ and $Fe-C^{\delta2}$ distances than on the $Fe-N^{\delta1}$ and $Fe-C^{\gamma}$ distances and that the internal ring vibrations have low amplitudes.[36]

The heme in both models was constrained to be planar. Unless this was done, the calculations produced implausible distortions. During the initial refinement cycles for the PP-IX model, it was observed that differences among the four $Fe-N_p$ distances were ≤0.01 Å. To reduce the number of degrees of freedom in the model even further, the four $Fe-N_p$ distances were constrained to be equal. In the TPP model, the heme was constrained to be symmetric with respect to the four mirror planes perpendicular to the heme (Figures 2 and 3a, Table 2). Except where stated, the imidazole ring was constrained to lie in the plane perpendicular to the heme and passing through N^A-Fe-N^C ("eclipsed"). No significant changes were observed when the imidazole was constrained to lie in the plane perpendicular to the heme and passing through the *meso*-C's ("staggered"), i.e., bisecting the angle between N^A-Fe-N^C and N^B-Fe-N^D (Figure 2). The bond lengths and internal bond angles of the imidazole group were restrained to their normal

(34) The limit of 5.1 Å was chosen to include a potentially significant path, $Fe\rightarrow N^A\rightarrow C^{4C}\rightarrow Fe$, with effective length ∼5.07 Å, degeneracy 16, and importance factor ∼23%. The most significant six-leg path was $Fe\rightarrow N^C\rightarrow C^{1C}\rightarrow N^C\rightarrow C^{1C}\rightarrow N^C\rightarrow Fe$, with effective length ∼4.80 Å, degeneracy 8, and importance factor ∼8.6%.

(35) Ellis, P. J. Ph.D. Thesis, University of Sydney, 1995.
(36) Pettifer, R. F.; Foulis, D. L.; Hermes, C. *J. Phys. (Paris)* **1986**, *47*, 545−550.

values (Figure 3b), while the Debye−Waller factors, for $C^{\delta 2}$ and $C^{\epsilon 1}$ were constrained to be equal, as were those for C^{γ} and $N^{\delta 1}$. The two Fe−N−C angles at the imidazole $N^{\epsilon 2}$ atom were restrained to be equal with an esd of 2°. For met-Mb, the Fe atom was constrained to lie in the porphyrin plane, consistent with the reported small deviations (0.16, 0.03 Å) from the porphyrin plane in the crystal structures of sperm whale and horse heart met-Mb.[6] In the model for deoxy-Mb, the Fe atom was constrained to lie 0.3 Å from the porphyrin plane on the proximal side, again consistent with the deviation (0.3 Å) in the crystal structure of sperm whale deoxy-Mb.[6] The calculations for deoxy-Mb were repeated with models in which the Fe atom was constrained to distances 0.1, 0.2, and 0.3 Å on either side of the heme plane (see Table S1, Supporting Information).

Both met-Mb and deoxy-Mb were subjected to an additional MS refinement in which the axial Fe−L bond lengths were constrained to values derived from recent XRD structure analyses.

Reconstitution of Published XAFS Data for Sperm Whale Deoxymyoglobin. A published XAFS curve for sperm whale deoxy-Mb[22] was scanned at a resolution of ∼300 dpi by means of the program DataThief[37] to yield 102 data points in the range $1.0 \leq k \leq 11.8$ Å^{-1}. These data were used in a re-refinement of the Fe site, using the same MS protocol and starting model as for horse heart deoxy-Mb.

Results

Pre-Edge Features, XANES, and Protein Photodamage. As expected, the edge for deoxy-Mb occurs at much lower energy than that of met-Mb. The forbidden s → d transitions occur as weak doublet pre-edge peaks due to promotion of the electron into the partially filled t_{2g} and e_g orbitals, which are partially filled in the high-spin d^6 (deoxy) and high-spin d^5 (met) electronic configurations. These peaks have lower energies and higher intensities for the deoxy form than for the met form (Figure 4a).

Since the position and structure of the edge spectrum are sensitive indicators of the reduction of met-Mb to deoxy-Mb,[38] they were monitored during the collection of the data for met-Mb. The effect of irradiation was negligible during the first three scans in each position of the sample but became significant after that. When the data for all 22 scans (collected for two met-Mb samples at two positions each) were averaged, there was clear evidence for a shift to lower energy in comparison with the average of the first three scans in each position of the sample (Figure 4b). It was assumed that the photoreduced species was deoxy-Mb or a photodamaged species with a similar edge position, in which case the overall shift in the edge corresponded to a change of ∼6%. The data later used to refine the model for met-Mb were, therefore, limited to the average of the 12 scans that were affected least by photoreduction. The average edge shift in these 12 scans compared to the first scan corresponded to 2% reduction. No photodamage was detected in the edge data obtained from deoxy-Mb solutions.

Error Estimates. The probable errors in the Fe−L bond lengths were estimated as $[\sigma_r^2 + \sigma_s^2]^{1/2}$, where σ_r and σ_s represent contributions from the random and systematic errors, respectively. The random (statistical) errors due to noise in the data were estimated by Monte Carlo calculations,[27] and the systematic errors were assigned a conservative consensus value, 0.02 Å.[15] In the MS refinement of met-Mb, the calculated statistical errors were 0.007 Å for Fe−N_p, 0.014 Å for Fe−N_ϵ, and 0.024 Å for Fe−O. In the refinement of deoxy-Mb, the statistical errors were 0.002 Å for Fe−N_p, and 0.015 Å for Fe−N_ϵ. The resulting probable errors in the Fe−ligand bond lengths were in the range 0.02−0.03 Å (Table 4). For example, the probable error in the Fe−O distance in met-Mb was calculated as $[(0.024)^2 + (0.02)^2]^{1/2} \approx 0.03$ Å.

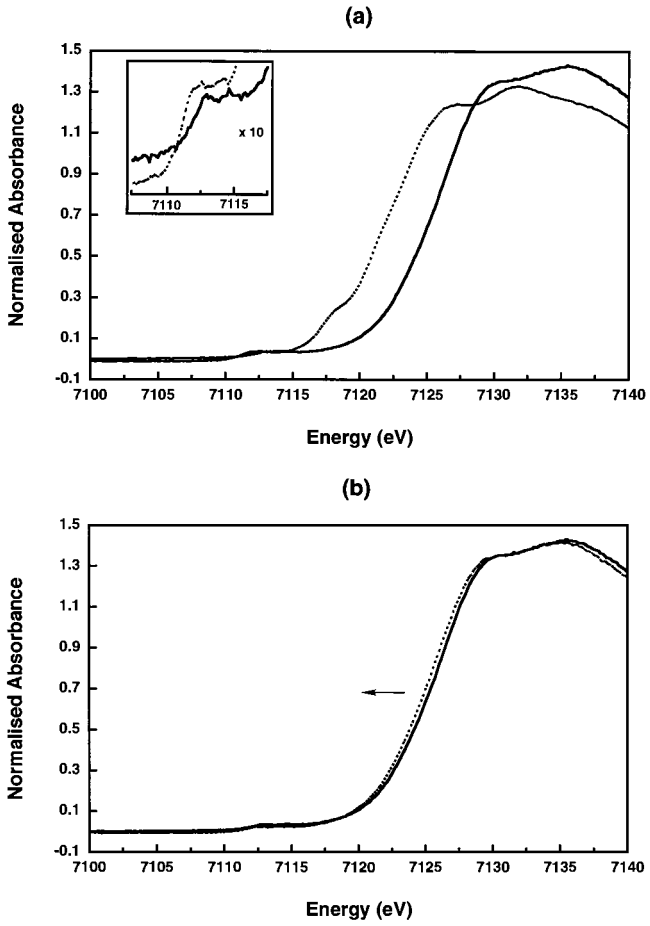

Figure 4. X-ray absorption edges: (a) average of 12 scans for met-Mb (first three scans in each of two positions of two specimens) (—) compared with deoxy-Mb (···); (b) average of 12 (—) and all 22 scans (···) for met-Mb.

XAFS Structures. The observed and calculated XAFS, $\chi(k) \times k^3$, for met- and deoxy-Mb, the corresponding Fourier transforms, the residuals, $\Delta[\chi(k) \times k^3]$, and the window functions used in the Fourier filter for met- and deoxy-Mb are shown in Figures 5 and 6, respectively. The refined structures of met- and deoxy-Mb are shown in Figure 7. The mean Fe−N_p distance and the Fe−N_ϵ distance found in the MS analysis are effectively the same as those from an SS analysis (Table 4), but the Fe−O bond length from the MS analysis is 0.11 Å longer. Differences between corresponding bond lengths derived from the refinement of the PP-IX and TPP models are not significant. Similarly, for met-Mb, data averaged over 12 scans gave the same bond lengths within experimental error, although the Debye−Waller factors were a little higher for the 22-scan data. The goodness-of-fit values, *R*, for the TPP model are slightly lower (met-Mb [22-scan data] 17.7%; met-Mb [12-scan data] 18.8%; deoxy-Mb 17.8%) than those for the PP-IX model (met-Mb [22-scan data] 20.9%; met-Mb [12-scan data] 20.8%; deoxy-Mb 19.4%).

Tests for Residual Errors in the Refined Models. In the XAFS analyses of both met- and deoxy-Mb (Figures 5 and 6), there appear to be significant residuals $\Delta[\chi(k) \times k^3]$ in the low-*k* region. In the Fourier transforms, these translate into residual amplitudes at distances corresponding to the second and third

(37) Huyser, K.; van der Laan, J. DataThief, v. 1.0.8; The National Institute for Nuclear Physics and High Energy Physics: Amsterdam, 1992.
(38) Penner-Hahn, J. E.; Hodgson, K. O. In *Iron Porphyrins, Part III*; Lever, A. B. P., Gray, H. B., Eds.; VCH Publishers: New York, 1989; Vol. 4, Chapter 3, and references therein.

Table 4. Fe-site Dimensions in Horse Heart and Sperm Whale Mb As Determined by MS and SS XAFS Analyses

		distances (Å)			Debye−Waller factors σ^2 (Å^2)			other refinement params			
protein	method	Fe−N_p	Fe−N_ϵ	Fe−O	N_p	N_ϵ	O	E_0 (eV)	S_0^2	R (%)	ref
met-Mb											
horse heart	SS[a,b]	2.06	2.18	1.97	0.001	0.010	0.010	7122.2	0.89	17.5	this work
horse heart	SS[a,c]	2.05	2.19	2.08	0.002	0.001	0.005	7127.1	1.0	21.8	this work; TPP model
horse heart	MS[a]	2.04(2)	2.16(2)	2.09(2)	0.001	0.001	0.001	7127.1	0.91(3)	20.8	this work; PP-IX model
horse heart	MS[a]	2.05(2)	2.17(2)	2.08(3)	0.002	0.001	0.001	7127.5	0.93(2)	18.8	this work; TPP model
sperm whale	SS	2.04(2)	2.11(2)	1.88(2)							39, 40
deoxy-Mb											
horse heart	SS[b]	2.07	2.18		0.002	0.011		7121.8	0.84	21.4	this work
horse heart	MS	2.06(2)	2.16(2)		0.002	0.001		7124.7	0.94(3)	19.4	this work; PP-IX model
horse heart	MS	2.06(2)	2.16(3)		0.002	0.001		7125.4	0.97(3)	17.8	this work; TPP model
sperm whale	SS	2.06(2)	2.12(2)								39, 40
sperm whale	SS[d]	2.07(2)									22
sperm whale	MS	2.06(2)	2.11(3)		0.003	0.001		7124.9	0.95	22.0	this work; data from ref 22

[a] Data from 12-scan average (see text). [b] Refinement using only the first shell. [c] Refinement with all of the shells used in the MS refinement, but only paths with two legs were considered. [d] Refinement with single Fe−N distance.[22]

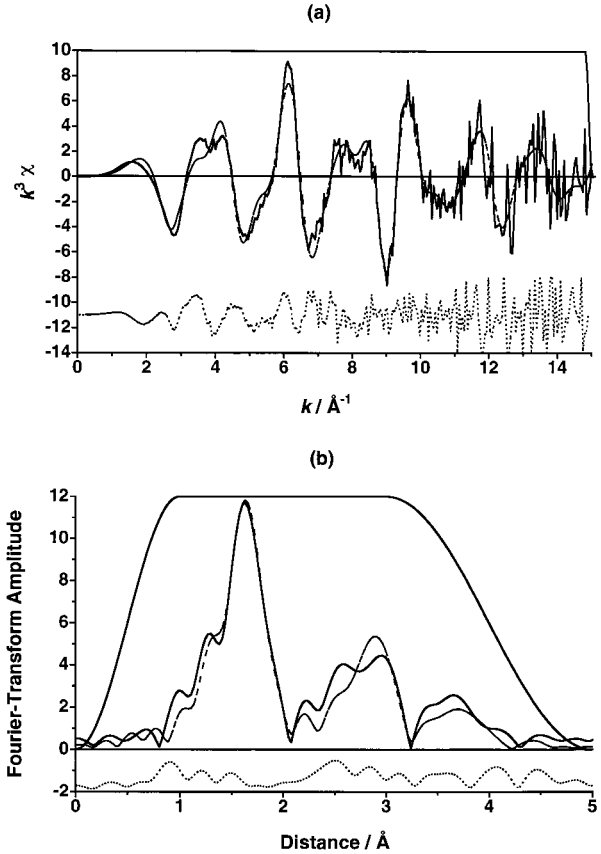

Figure 5. (a) XAFS and (b) Fourier transform amplitudes of XAFS for met-Mb: observed (—), calculated from refined model (- - -); residual (···); window used in Fourier filter (—).

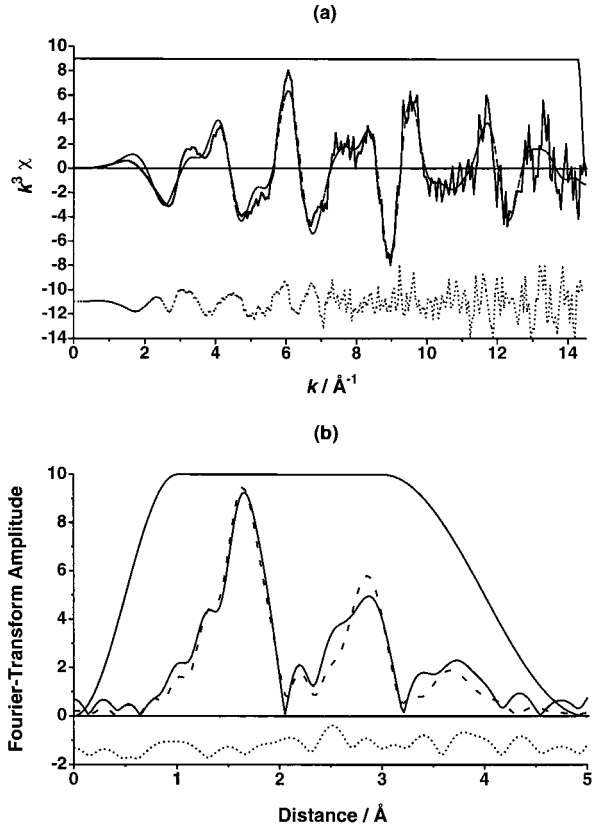

Figure 6. (a) XAFS and (b) Fourier transform amplitude of XAFS of deoxy-Mb: observed (—); calculated from refined model (- - -); residual (···); window used in Fourier filter (—).

shells. Two possible ways to improve the model were investigated. First, the imidazole ring was allowed to tilt by up to 30° perpendicular to its plane or rotate up to 30°. The improvements in the fit to the data were marginal, and the changes were limited to distances beyond the first shell, so that the Fe−L bond lengths were unaffected (Table S2, Supporting Information). Second, to obtain a better fit to the second shell of the Fourier transform, a sixth ligand was incorporated into the refinement for deoxy-Mb. In the structure of sperm whale deoxy-Mb,[6] the N_ϵ of the distal histidine is ∼4.6 Å from the Fe and the nearest water is ∼3.8 Å from the Fe. Therefore, two refinements were performed where either oxygen or the ImH ring of histidine was present on the distal side of the heme (see Table S1 and Figures S1 and S2, Supporting Information). The resulting bond lengths were 2.20 and 3.66 Å for the $O(OH_2)$ and N_ϵ(distal His) atoms, respectively. Neither the Fe−L bond lengths nor the refinement parameters altered significantly for the refinement with oxygen as the sixth ligand; however R improved by ∼1% (R = 16.5%). The Debye−Waller temperature factor for the $O(OH_2)$ atom was 0.009 Å^2, which is a reasonable value for a long Fe−O bond. The refinement also improved when the distal ImH ring was included in the refinement (R decreased to 15.4% when Fe−N_ϵ(distal) refined to 3.66 Å). The Fe−L bond lengths were not altered. The Debye−Waller temperature factor for the N_ϵ(distal) atom was much lower than expected for a long absorber−scatterer distance (0.001 Å^2).

Effect of the *k* Range on the Refinement. To determine the effect of truncating the k range used in MS analyses, and to

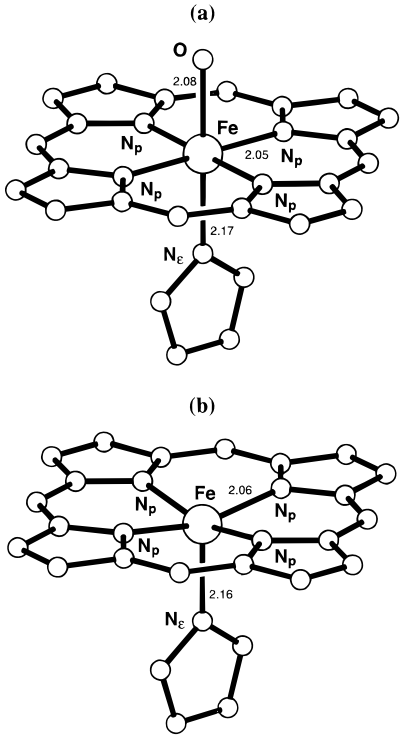

Figure 7. XAFS values for Fe−ligand bond lengths in (a) met- and (b) deoxy-Mb at 10 K.

provide a basis for comparisons with our MS reanalysis of sperm whale deoxy-Mb using published data with a more limited *k* range,[22] the refinement of horse heart deoxy-Mb was repeated with data up to $k = 11.0$, 12.0, 13.0, and 14.0 Å^{-1}. The Fe−N_ϵ bond distance increased from 2.13 to 2.16 Å when the upper limit of *k* was raised from 11.0 to 14.0 Å^{-1} and then remained constant at 2.16 Å when the data to $k = 15.0$ Å^{-1} were included. The average Fe−N_p bond length (2.06 Å) was unaffected by the *k* range.

Effect of Long Multiple-Scattering Paths. During a systematic exploration of the effects of restricting the number of multiple-scattering MS paths (see Experimental Section), it was observed that even distant shells can make a significant contribution to the XAFS if the degeneracy of the MS paths is high. Heme proteins provide opportunities for such MS paths. For example, SS paths with an effective length as large as 4.28 Å (the 8-fold degenerate Fe→C_β→Fe path) can have an importance factor as great as 32% of that of the most important contribution (i.e., the 4-fold degenerate Fe→N_p→Fe path). Details of MS paths and their importance factors have been deposited as Supporting Information.

XAFS Contributions of Axial Ligands. At the conclusion of an MS refinement of met-Mb in which the Fe atom was constrained to the porphyrin plane, the imidazole and water ligands were moved along the normal to the porphyrin plane so that the Fe−N_ϵ(imidazole) and Fe−O(aqua) distances were interchanged. The MS refinement was then continued until convergence was again reached. The refinement converged to the original minimum ($R = 18.8\%$, Fe−N_p = 2.05 Å, Fe−N_ϵ = 2.17 Å, and Fe−O = 2.08 Å; Table S1, Supporting Information), showing that the two axial ligands make distinct MS contributions to the XAFS.

Distance of the Fe Atom from the Porphyrin Plane. The axial Fe−ligand bond lengths in met-Mb were affected by the position of the Fe atom in relation to the porphyrin plane. The results cited in Table 4 are based on an MS refinement in which the Fe was constrained to lie within the porphyrin plane (see "Constraints and Restraints", above). Neither the Fe−ligand bond lengths nor the goodness-of-fit parameter *R* changed significantly when the Fe atom was constrained to be 0.1 or 0.2 Å from the heme plane on the distal side (Table S1, Supporting Information). However, when the structure was refined with the Fe atom constrained to a position 0.1 Å out of the porphyrin plane on the proximal side, the axial Fe−ligand bond lengths became approximately equal; and when the refinement was repeated with the distance of the Fe atom from the porphyrin plane increased to 0.2 Å on the proximal side, the axial Fe−ligand bond lengths were reversed. Neither the Fe−N_p bond lengths nor the residual *R* factors were altered significantly (18.8 ± 0.5%).

In contrast with those in met-Mb, the Fe−ligand bond lengths in deoxy-Mb were insensitive to the distance of the Fe atom from the porphyrin plane (Table S1, Supporting Information). Within the estimated limits of precision, MS refinements with the Fe atom constrained to a position 0.3, 0.2, or 0.1 Å from the porphyrin plane on the distal or proximal side produced the same values for the Fe−N_p and Fe−N_ϵ(imidazole) bond lengths. The values of the goodness-of-fit parameter *R* also showed little variation (17.3 ± 0.4%).

Multiple-Scattering Refinement of the Fe Site in Sperm Whale Deoxymyoglobin. An MS refinement of the Fe site in sperm whale deoxy-Mb, using published XAFS data in the range $1.0 \le k \le 11.8$ Å^{-1}, yielded the dimensions Fe−N_p(av) = 2.06 Å and Fe−N_ϵ = 2.11 Å. These values were not significantly different from those obtained for horse heart deoxy-Mb, Fe−N_p = 2.06 Å and Fe−N_ϵ = 2.13 Å, using data in the same *k* range.

Single-Scattering Refinements of the Fe Site in Horse Heart Met- and Deoxymyoglobin. Using conventional SS calculations, the XAFS data recorded for met-Mb in the present work could be fitted equally well by a first shell comprising six equal Fe−N bond lengths, one Fe−O, and five equal Fe−N bond lengths or several combinations of Fe−N_p, Fe−N_ϵ, and Fe−O bond lengths (Table S3, Supporting Information). The average Fe−L bond lengths produced by all these SS refinements, 2.05−2.07 Å, were the same within the estimated limits of precision. When the Fe−N_p distance was treated as a separate variable, the resulting value was within 0.02 Å of the values found in previous SS analyses,[22,39,40] but the Fe−N_ϵ and Fe−O bond lengths were dependent on the starting distances of the model (Table S3, Supporting Information). In the case of deoxy-Mb, the SS results did not differ significantly from the MS results for the Fe−L bond lengths.

Discussion

Edge and Pre-Edge Features. The edge (XANES) and pre-edge features of the proteins provide information about the symmetry, spin state, and oxidation state of the metal ion. The derivation of structural information from the XANES, on the other hand, is more difficult and open to uncertainty than the MS analysis of XAFS data. The following discussion is restricted to a qualitative analysis of the XANES region.

While the edge energies of a variety of high-spin and low-spin six-coordinate Fe(III) heme proteins lie in a range of <1

(39) Chance, B.; Fischetti, R.; Powers, L. *Biochemistry* **1983**, *22*, 3820−3829.
(40) Powers, L.; Sessler, J. L.; Woolery, G. L.; Chance, B. *Biochemistry* **1984**, *23*, 5519−5523.

eV, the edge energies for six-coordinate Fe(II) heme proteins are about 3 eV higher than that for deoxy-Mb.[41,42] This difference is probably associated with the lower coordination number and coordination symmetry of Fe(II) in deoxy-Mb, the symmetry being reduced not only by the loss of a ligand but also by the movement of the Fe atom out of the porphyrin plane. The lowering of the coordination symmetry also accounts for the fact that deoxy-Mb has more intense pre-edge features than met-Mb. The pre-edge features are due to the symmetry-forbidden $s \rightarrow d(t_{2g},e_g)$ transitions. Their intensities are derived from a relaxation of the selection rules due to mixing of the p and d orbitals.[43] The orbital mixing is increased when the symmetry of the complex is reduced and/or the Fe moves out of the porphyrin plane for the deoxy form of the protein.

Accuracy and Precision of the Fe−L Bond Lengths from XAFS and X-ray Crystallography. The crystal structure analysis of sperm whale myoglobin played a seminal role in protein crystallography.[3] The discovery of the eight-helix polypeptide fold, the location of the heme group, the identification of the proximal histidine ligand, and the description of the heme pocket were just some of the revelatory aspects of the structure. The dimensions of the Fe site were not immediately accessible. A determination of these dimensions had to await the development of methods for the refinement of protein structures. The Fe−ligand bond lengths subsequently found by the refinement of the sperm whale and horse heart met- and deoxy-Mb structures are listed in Table 1. The spread among the values of each bond length reflects differences in the methodology of diffraction measurements and differences in the resolution of the data symptomatic of variation in crystal quality.

As a guide to the precision of the Fe−ligand bond lengths in Table 1, we have listed the diffraction precision indicator (DPI)[44] for each structure. The DPI has been proposed by Cruickshank as a function that reflects the quality of the diffraction data (resolution, completeness) as well as the quality of the refinement (excess of diffraction data over variable parameters, crystallographic residual). It provides an estimate of $\sigma_w(x)$, the uncertainty in the position of an average atom. Strictly speaking, the values of $\sigma_w(x)$ in Table 1 should be multiplied by $2^{1/2}$ in order to represent the estimated uncertainty in a bond length. We shall treat the "as calculated" $\sigma_w(x)$ as the quasi-esd of the Fe−ligand bond lengths, on the grounds that the values have been calculated in a doubly conservative way. First, we have used Cruickshank's value of 1.0 for the numerical factor in the expression for $\sigma_w(x)$. A value of 0.7 can be justified, but the conservative value is recommended to allow for the use of diagonalized-matrix instead of full-matrix least-squares refinement.[44] Second, the "average" atom to which $\sigma_w(x)$ applies is an atom with an average displacement factor ("temperature factor"). The atoms at the metal site of a metalloprotein generally have below-average temperature factors, in which case an empirical correction leads to below-average values of $\sigma_w(x)$. We have listed the "global" values of $\sigma_w(x)$ in Table 1, since some of the data required for the modified expression are not currently available. The general conclusion from Table 1 is that the best of the horse heart and sperm whale Mb crystal structures have Fe−ligand bond length esd's of ~0.1 Å. The esd's are in fact sufficiently large that, despite the range of

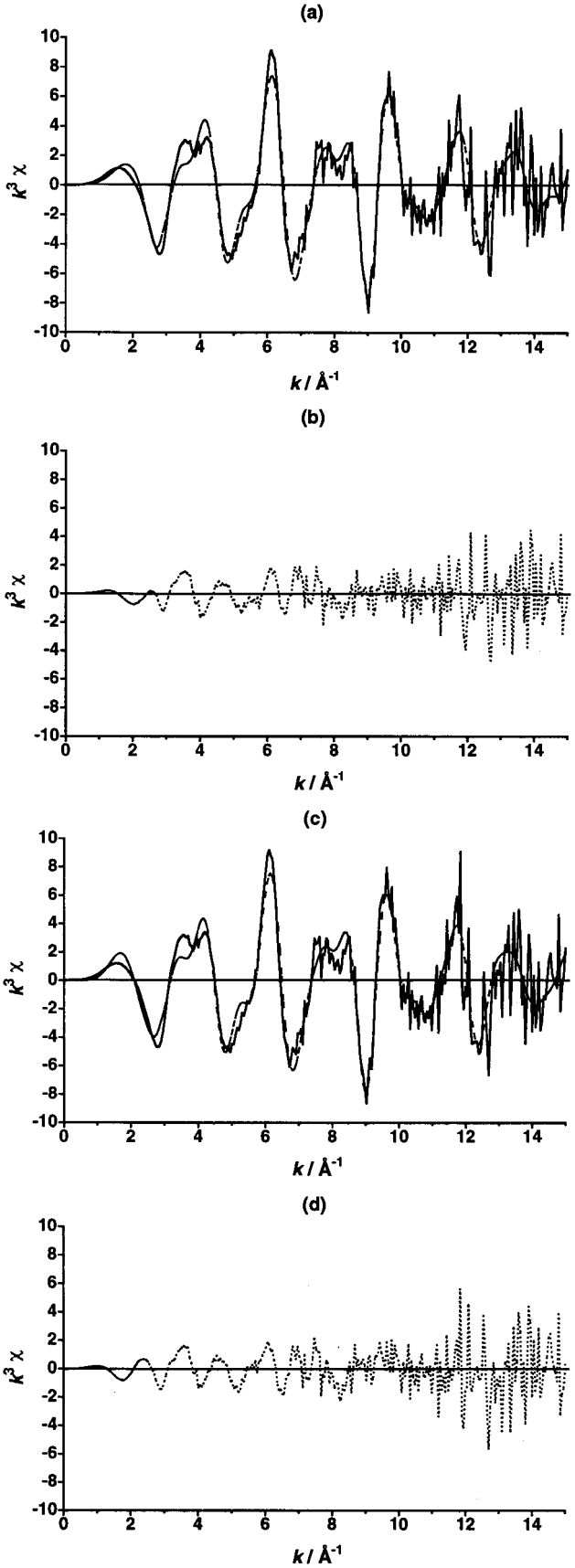

Figure 8. Observed (—) and calculated (- - -) XAFS for met-Mb: (a) unconstrained Fe−L bond lengths; (b) residual for (a); (c) axial bond lengths constrained to the crystallographic values in horse heart met-Mb,[8] Fe−N_ϵ = 2.26 Å and Fe−O = 2.29 Å; (d) residual for (c).

(41) Rich, A. M. Ph.D. Thesis, University of Sydney, 1997.
(42) Rich, A. M.; Armstrong, R. S.; Ellis, P. J.; Lay, P. A. *J. Am. Chem. Soc.*, in press.
(43) Westre, T. E.; Kennepohl, P.; DeWitt, J. G.; Hedman, B.; Hodgson, K. O.; Solomon, E. I. *J. Am. Chem. Soc.* **1997**, *119*, 6297−6314.
(44) Cruickshank, D. W. J. In *Macromolecular Refinement. Proceedings of the CCP4 Study Weekend, January 1996*; Dodson, E., Moore, M., Ralph, A., Bailey, S., Eds.; SERC Daresbury Laboratory: Warrington, U.K., 1996; pp 11−22.

Table 5. Multiple-Scattering XAFS Refinements of Horse Heart met- and deoxy-Mb, Showing the Effects of Constraining the Axial Fe−L Bond Lengths to Unusual Values from XRD Structure Analyses of Horse Heart met-Mb[8] and Sperm Whale deoxy-Mb[7]

		distances (Å)			Debye−Waller factors σ^2 (Å^2)			other refinement params		
protein	constraints (Å)	Fe−N_p	Fe−N_ϵ	Fe−O	N_p	N_ϵ	O	E_0 (eV)	S_0^2	R (%)
met-Mb	nil	2.05(2)	2.17(2)	2.08(3)	0.002	0.001	0.001	7127.5	0.93(2)	18.8
	Fe−N_ϵ = 2.26 + Fe−O = 2.29	2.07	2.26	2.29	0.003	0.04	0.04	7127.4	1.37	22.0
deoxy-Mb	nil	2.06(2)	2.16(3)		0.002	0.001		7125.4	0.97(3)	17.8
	Fe−N_ϵ = 2.30	2.07	2.30		0.003	0.07		7125.0	1.21	18.7

values for each bond length, none of the bond lengths differ significantly from the values found by XAFS (Table 4).

For the XAFS-derived Fe−ligand bond lengths listed in Table 4, we have calculated probable errors as already described (see "Error Estimates", above). The estimates take into account both random and systematic errors but are dominated by the latter. Using a consensus value of 0.02 Å for the systematic error component, we obtain overall probable errors in the range 0.02−0.03 Å for the Fe−ligand distances derived from the MS XAFS analyses. Thus, there is an improvement by factors of 3−5 over the precision of the best crystallographically determined Fe−ligand bond lengths available at this time.

The validity of the MS procedures used here has been verified elsewhere by determining the structure of [Fe(TPP)(NO)] by MS analysis of XAFS data and showing that the Fe−L bond lengths thus determined were within experimental error of with its precise X-ray structure.[41,42] The ability of MS methodology the model to reproduce Fe−L bond lengths of a well-defined model complex, within experimental error, supports the conclusions drawn about the precision of such bond lengths for the heme proteins. The extent to which restraints placed on the Debye−Waller factors may affect the accuracy of the analyses has also been considered. The refined Debye−Waller values are all reasonable and lower than the maximum value of the restraint. It is, therefore, unlikely that these restraints have biased the results of the analysis.

Comparisons with Previous XAFS Studies of Myoglobin. The present work pinpoints a number of factors that may have limited the accuracy of previous XAFS determinations of the Fe−ligand bond lengths in Mb. These include the use of XAFS data in a smaller k range, the effects of photodecomposition, and the use of SS instead of MS analyses.

The effects of using a limited k range were seen clearly when the structure of deoxy-Mb was refined using XAFS data with different values of k_{max} (see "Effect of the k Range", above). While the Fe−N_p bond length was unaffected, the use of data with $k_{max} < 14$ Å^{-1} led to a systematic decrease in the axial Fe−N_ϵ bond length. Photoreduction may be a more serious problem. During the collection of XAFS data at 10 K, we observed photodamage to met-Mb even during relatively short exposures. It has been shown elsewhere that when photoreduction exceeds about 10%, the accuracy of heme protein MS analyses is significantly compromised.[41,42] Accordingly, the data used to refine the met-Mb Fe−ligand bond lengths in the present work were restricted to scans where the level of photoreduction averaged 2%. There appears to be no published record that photoreduction of met-Mb was noticed in previous XAFS studies.[39,40] The possibility of similar effects during prolonged exposures of met-Mb crystals to synchrotron radiation for XRD measurements, especially at ambient temperature,[8,45] should be considered.

The importance of using an MS rather than an SS analysis is illustrated by our results for met-Mb, where the use of SS led to significant errors in the axial Fe−ligand bond lengths. The lower accuracy of the SS results when fitted to a three-shell model and the apparent inconsistencies among the previous SS XAFS studies of Mb[39,40] are explained by the fact that the resolution of distances in an SS analysis depends on $\pi/2\Delta k_{max}$. Thus SS XAFS analyses cannot distinguish with certainty between distances that differ by 0.14 Å at $k_{max} = 11$ Å^{-1} or 0.11 Å at $k_{max} = 14.5$ Å^{-1}.[46,47]

Met-Mb. The XAFS-derived Fe−N_p, Fe−N_ϵ, and Fe−OH_2 bond lengths shown in Table 4 (2.04(2), 2.16(2), and 2.08(3) Å) are in good agreement with the average bond lengths obtained from the best three XRD structures in Table 1 (Fe−N_p = 2.01 Å, Fe−N_ϵ = 2.14 Å, Fe−O = 2.13 Å).[4,7] The Fe−N_p and Fe−OH_2 bond lengths are also consistent with the bond values 2.045(8) and 2.095(2) Å determined by XRD for the high-spin distorted-octahedral model complex $[Fe(TPP)(OH_2)_2]^+$.[48] The MS analysis was able to distinguish between the Fe−N_ϵ and Fe−OH_2 bonds, since a refinement with the Fe constrained to the heme plane and with the axial bond lengths initially interchanged reverted to the correct final structure (see "XAFS Contributions of Axial Ligands", above). The MS analysis was relatively insensitive to displacement of the Fe atom from the heme plane (i.e., toward the OH_2 ligand), but the axial bond lengths became reversed if the Fe was constrained to lie 0.2 Å from the heme plane on the proximal side (see "Distance of the Fe Atom from the Porphyrin Plane", above). However, the distance required to reverse the axial bond lengths (0.2 Å) is unrealistic for a six-coordinate complex. For instance, the Fe atom is in the plane for the high-spin $[Fe(TPP)(OH_2)_2]^+$ complex.[48] This shows that the porphyrin ring is able to accommodate the "long" Fe−N_p bond lengths found in the high-spin complexes.

The present results for met-Mb disagree both with an earlier XAFS determination where the Fe−OH_2 bond in sperm whale met-Mb was reported as being very short (1.88 Å)[22,39] and with two XRD analyses where both axial bonds were reported as being very long (2.50, 2.25 Å and 2.26, 2.29 Å).[7,8] The discordant very low XAFS value for the Fe−OH_2 bond can be disregarded on the grounds that it was derived from an SS analysis using very limited data ($k_{max} = 12.5$ Å^{-1}). The two crystal structures with very long axial bonds can also be discounted, since they have such large $\sigma_w(x)$ values that the differences from the XAFS values are within the limits of

(45) Evans, S. V.; Brayer, G. D. *J. Biol. Chem.* **1988**, *263*, 4263−4268.

(46) Riggs-Gelasco, P. J.; Stemmler, T. L.; Penner-Hahn, J. E. *Coord. Chem. Rev.* **1995**, *144*, 245−286, and references therein.

(47) In SS calculations, a window is frequently used to limit the data to a range in which only the backscatterers bound to the absorber (here, the Fe center) contribute. We thank a reviewer for pointing out that a more valid comparison with the MS results would be obtained if the SS data represented all of the backscatterers that were included in the MS analysis. We performed such an SS analysis for met-Mb, using all of the data and the same number of atoms as in the MS analysis. The resulting bond lengths were consistent with those shown in Table 4 for the MS analysis, but the value of R was significantly higher (21.8% compared with 18.8%) and some of the Debye−Waller factors were so high that the relevant backscatterer was effectively eliminated (e.g., 0.08 for the C^β atoms of the porphyrin).

(48) Scheidt, W. R.; Cohen, I. A.; Kastner, M. E. *Biochemistry* **1979**, *18*, 3546−3552.

precision. Nevertheless, we have tested the hypothesis that the long axial bonds are consistent with the XAFS data by repeating the MS XAFS refinement with the Fe−N_ϵ and Fe−OH_2 bond lengths constrained to 2.26 and 2.29 Å, respectively. Although a quantitatively reasonable fit to the observed XAFS was obtained (Figure 8), the goodness-of-fit *R* increased by ∼3%, the scale factor S_0^2 increased from its normal value of 0.9−1.0 to an unreasonable value of 1.4, and the axial donor atoms N_ϵ and O had Debye−Waller factors of $\sigma^2 = 0.04$ Å^2 so that their contributions to the XAFS were reduced almost to zero (Table 5). We conclude that the long axial Fe−ligand bonds found in two of the crystal structure analyses of met-Mb are inconsistent with the XAFS data.

Deoxy-Mb. The Fe-site dimensions obtained by the XAFS refinement of horse heart deoxy-Mb differ from the results for met-Mb in two ways. First, the SS and MS analyses yielded identical Fe−ligand distances (Fe−N_p = 2.06(2) Å, Fe−N_ϵ = 2.16 Å) within the limits of precision (Table 4). Second, the results were insensitive to displacements of the Fe atom from the porphyrin plane by ≤0.3 Å (Table S1, Supporting Information, and "Distance of Fe Atom from Porphyrin Plane", above). For example, constraining the Fe atom to lie 0.2 Å from the porphyrin plane on the distal side produced the best goodness-of-fit (16.9%) but left the Fe−ligand bond lengths unchanged. The reason for this lack of sensitivity is that displacements of the Fe atom from the porphyrin plane cause only small changes in the N_p−Fe−N_ϵ and N_p−Fe−N_p angles and, hence, in the MS paths.[49] The effect of similar displacements in met-Mb paths is more pronounced, due to the additional MS paths generated by the presence of the O(water) scatterer and the approximately linear arrangement of O−Fe−N_ϵ.

The present work reaffirms the conclusion from an earlier debate[50−53] that XAFS alone does not yield an accurate value for the displacement of the Fe atom from the porphyrin plane in deoxy-Mb. A displacement of 0.3 ± 0.05 Å in sperm whale deoxy-Mb and in human deoxyhemoglobin has been deduced from XANES data.[51,54] We have not replicated the detailed XANES analysis, since the edge and pre-edge features in our spectra for horse heart deoxy-Mb are closely similar to the published observations for related proteins.[51,54] The similarity in the spectra suggests that the Fe in horse heart deoxy-Mb is also displaced from the heme plane.

To the best of our knowledge, the only previous XAFS studies of deoxy-Mb were SS analyses of the sperm whale protein using data to k_{max} = 12.5 Å^{-1}.[22,39,40] The Fe−ligand bond lengths now reported for horse heart deoxy-Mb are in general agreement with the earlier results, as well as with a MS reanalysis of the XAFS data reported in 1991[22] (Table 4). The difference between the new value for the Fe−N_ϵ bond length (2.16(2) Å) and the values derived from the earlier analyses (2.12, 2.11 Å) is due to the improved *k* range of the present data. We have shown this by repeating our MS analysis of horse heart deoxy-Mb, using a truncated data set. Reducing the *k* range of the horse heart deoxy-Mb data to k_{max} = 11.8

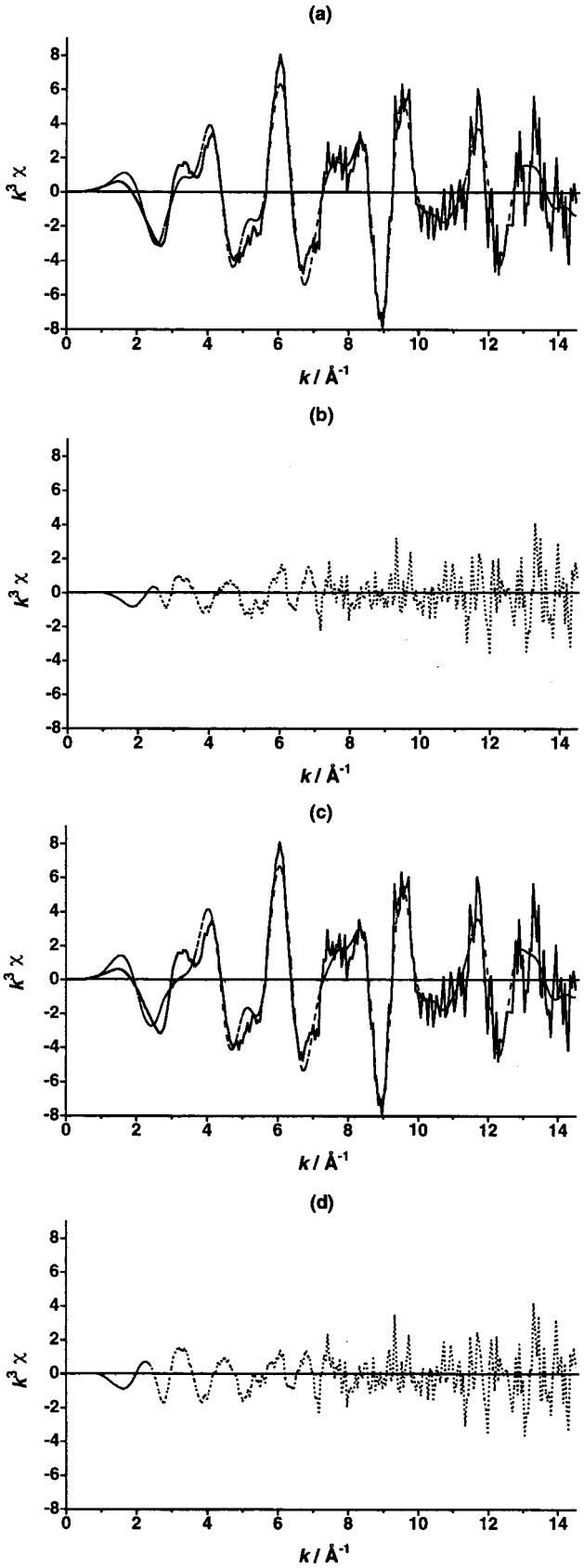

Figure 9. Observed (—) and calculated (- - -) XAFS for deoxy-Mb: (a) unconstrained Fe−L bond lengths; (b) residual for (a); (c) axial Fe−N_ϵ bond length constrained to a recent crystallographic value,[7] 2.30 Å; (d) residual for (c).

(49) Westre, T. E.; Cicco, A. D.; Filipponi, A.; Natoli, C. R.; Hedman, B.; Solomon, E. I.; Hodgson, K. O. *J. Am. Chem. Soc.* **1994**, *116*, 6757−6768.
(50) Bolton, W.; Perutz, M. F. *Nature (London)* **1970**, *228*, 551−552.
(51) Perutz, M. F. *Nature (London)* **1970**, *228*, 726−734.
(52) Eisenberger, P.; Shulman, R. G.; Kincaid, B. M.; Brown, G. S.; Ogawa, S. *Nature (London)* **1978**, *274*, 30−34.
(53) Bianconi, A.; Congiu-Castellano, A.; Dell'Ariccia, M.; Giovannelli, A.; Durham, P. J.; Burattini, E.; Barteri, M. *FEBS Lett.* **1984**, *178*, 165−170.
(54) However, the authors[53] observed that "other possible distortions of the heme can also affect the XANES in a similar way".
(55) Bernstein, F. C.; Koetzle, T. F.; Williams, G. J. B.; Meyer, E. F., Jr.; Brice, M. D., Jr.; Rodgers, J. R.; Kennard, O.; Shimanouchi, T.; Tasumi, M. *J. Mol. Biol.* **1977**, *112*, 535−542.

$Å^{-1}$ resulted in a reduction of the Fe−N_ϵ bond length from 2.16 to 2.13 Å.

XRD analyses of deoxy-Mb have been published only for the sperm whale protein (Table 1). The Fe-site dimensions (Fe−N_p = 1.95−2.07 Å, Fe−N_ϵ = 2.10−2.31 Å) have sufficiently large values of the quasi-esd $\sigma_w(x)$ to render differences from the present XAFS results insignificant within the limits of precision. As in the case of met-Mb (see above), the two largest values of the Fe−N_ϵ bond length were tested by performing an MS XAFS refinement in which the axial bond was constrained to 2.3 Å. The agreement between the observed and calculated XAFS again remained qualitatively reasonable (Figure 9), and the goodness-of-fit value increased by only 0.9%. However, the scale factor S_0^2 increased from 0.97 to 1.21, and the Debye−Waller factor $\sigma^2 = 0.07$ Å effectively eliminated the contribution of the axial N_ϵ scatterer to the XAFS (Table 5). The hypothesis that a 2.3-Å Fe−N_ϵ bond is consistent with the XAFS data can therefore be dismissed with high probability.

Conclusions

This work provides examples of both the strengths and weaknesses of XAFS as a technique for the study of metalloproteins. The new values of the metal−ligand bond lengths in horse heart met- and deoxy-Mb have probable errors in the 0.02−0.03 Å range compared with esd's of ≥0.07 Å for similar bonds in well-refined crystal structures at 1.4−2.0 Å resolution. These new bond lengths have been obtained by MS calculations, using XAFS data recorded from frozen (10 K) solutions of the protein. In the case of horse heart met-Mb, the MS results are significantly different from those obtained when the model is fitted to the same data by SS calculations. It is no surprise that the values of some (but not all) of the metal−ligand bond lengths in Mb exhibit a systematic dependence on the *k* range of the XAFS data and that accurate results depend on the experimenter's ability to monitor and maintain the integrity of the protein sample.

The increasing understanding of these factors is accompanied by an increasing realization that significant problems remain to be overcome. These relate particularly to the effects of computational strategies that are invoked to overcome both practical and theoretical limitations of XAFS refinements. First, MS calculations on even a relatively simple metal site in a protein can generate so many paths that the calculations become, for practical purposes, impossibly lengthy. The experimenter must then apply software restrictions to ensure that only significant MS paths are considered. This type of decision is facilitated by the FEFF 6.01[26] program within the XFIT software package[27,28] used in the present work. Nevertheless, even the selection of cutoff limits involves subjective judgments, the effects of which have not yet been explored systematically. Second, it is frequently necessary to apply constraints to reduce the number of parameters that are fitted to the XAFS data (i.e., refined) and to apply restraints to prevent the generation of implausible structures. As in the refinement of macromolecular crystal structures, the weighting of the constraints and restraints in relation to the experimental data is largely arbitrary. While the experimenter may adopt empirical strategies to ensure that the constraints and restraints do not systematically affect the refined variables, the effect of the constraints and restraints on the estimation of errors is less clear. In the present work, we have emphasized this difficulty by referring to the estimated errors in crystallographically determined distances as esd's, while referring to the uncertainties in XAFS-derived distances as probable errors. Finally, the MS technique is not sufficiently sensitive to determine displacements of the Fe from the plane of the porphyrin or deviations of the porphyrin group from planarity. As indicated here and elsewhere,[41] physically reasonable values for such distortions do not change the Fe−L bond lengths and have little effect on the *R* values.

In light of our redetermination of the Fe−ligand distances in horse heart deoxy-Mb and met-Mb, we conclude the following: (i) MS XAFS analyses lead to Fe−ligand bond lengths that are more precise and accurate than those determined by SS XAFS analyses or protein crystallography. (ii) In structures such as heme proteins, where MS paths may have a large degeneracy, even distant shells can make a significant contribution to the XAFS. (iii) It is essential to monitor XAS and synchrotron XRD data for photodamage. (iv) The currently available XAFS data do not permit the displacement of the Fe atom from the heme plane in heme proteins to be determined accurately.

Acknowledgment. This work was supported by the Australian Nuclear Science and Technology Organization, Access to Major Facilities Program. A.M.R. is grateful for funding through an Australian Postgraduate Research Award and the James Kentley Memorial Traveling Scholarship. We thank Professor Keith Hodgson and Dr. Britt Hedman for assistance at SSRL, Dr. Simon Easterbrook-Smith, from the Department of Biochemistry at the University of Sydney, for final purification and concentration of the horse heart Mb, and Professor S. E. V. Phillips for supplying unpublished details of his protein crystallography data. Work was done (partially) at SSRL, which is operated by the Department of Energy, Office of Basic Energy Sciences. The SSRL Biotechnology Program is supported by the NIH, Biomedical Research Technology Program, National Center for Research Resources. Further support was provided by the Department of Energy, Office of Health and Environmental Research.

Supporting Information Available: Listings of the results of MS XAFS analyses of deoxy- and met-Mb with the Fe constrained to be at various distances from the porphyrin plane, effects of tilt and rotation of the plane of the proximal imidazole toward the porphyrin plane on the Fe−L bond lengths in horse heart met-Mb determined from MS XAFS, and SS results for met-Mb, a table and figures showing the results of MS XAFS analyses of deoxy-Mb in the presence of a sixth ligand (either OH_2 or distal imidazole), a table of the MS paths contributing to the XAFS refinement of met-Mb and their importance factors, tables of raw XAFS data, and a figure comparing the observed and Fourier-transformed XAFS for sperm whale deoxy-Mb from an earlier publication[22] with the results of the MS XAFS reanalysis (15 pages). Ordering information is given on any current masthead page.

IC9714549